J. Fluid Mech. (1994), *vol.* 259, *pp.* 125–148

Edge waves forced by short-wave groups

By HEMMING A. SCHÄFFER

Danish Hydraulic Institute, Agern Allé5, DK-2970 Hørsholm, Denmark

(Received 16 February 1993 and in revised form 29 June 1993)

On the basis of the theory for infragravity waves induced by short-wave groups developed by Schäffer (1993), three-dimensional infragravity waves are analysed. The theory relies on the linearized depth-integrated conservation equations for mass and momentum combined to give a second-order long-wave equation with forcing expressions in terms of the radiation stress. This forcing gives a dynamic set-up originating from oscillations of the break-point position and a dynamic set-down bound to the short-wave groups. For small angles of incidence leaky-mode solutions are found while trapped modes appear when the primary waves are sufficiently oblique. In the latter case resonant edge-wave excitation may occur. A semi-analytical steady-state solution for the infragravity motion is presented. The solution is restricted to periodicity along a plane beach connected to a shelf and valid only for small primary-wave modulations.

1. Introduction

It has been widely discussed in the literature whether *leaky modes* (as opposed to *trapped modes*, see e.g. Munk, Snodgrass & Carrier 1956) constitute the main part of infragravity wave motion, or if this is primarily an *edge wave* phenomenon.

Convincing field evidence for the presence of edge waves has been given by Huntley, Guza & Thornton (1981) and others. Using a complicated mathematical development Gallagher (1971) presented a theoretical model for edge-wave generation by different spectral components. Using a number of crude assumptions he was able to calibrate the model to give an approximate fit to some observed infragravity spectra.

In a lengthy WKB-expansion with multiple scales in time and offshore direction Foda & Mei (1981) treated the case of oblique incident short waves under the assumption that the long waves were of the same magnitude as the short waves. They obtained equations for the evolution as well as the interactions at different orders, and applied their derivations to the case of a closed coast, using empirical relations for the breaking of the short waves.

In Schäffer (1993, hereafter referred to as I) a mathematical model was formulated using the conservation equations for mass and momentum, which were previously used by for example Symonds, Huntley & Bowen (1982) and Mei & Benmoussa (1984). An essential feature was the special modelling of the forcing short-wave groups accounting for a time-varying break-point position in addition to the ordinary wave-group forcing. Solutions were only presented for strictly cross-shore motion whereas the present paper is concerned with obliquely incident wave groups.

The governing equations are given in §2 and a semi-analytical steady-state solution for the infragravity wave motion is developed in §3. Examples of the resulting surface elevation, the horizontal components of the infragravity particle velocity, and the mean infragravity-wave energy flux are presented in §4, where the effect of varying the input parameters is also analysed, focusing on the mechanism of edge-wave trapping.

2. Governing equations

The development of the governing equations is given in detail in I and we shall repeat them here with just a few comments. For a one-dimensional depth $h(x)$ the long-wave equation (2.9)[I]† reads in Cartesian coordinates (x, y) (neglecting bed friction)

$$\frac{\partial}{\partial x}\left(gh\frac{\partial\bar{\zeta}}{\partial x}\right)+gh\frac{\partial^2\bar{\zeta}}{\partial y^2}-\frac{\partial^2\bar{\zeta}}{\partial t^2}=-\frac{1}{\rho}\left(\frac{\partial^2 S_{xx}}{\partial x^2}+2\frac{\partial^2 S_{xy}}{\partial x\,\partial y}+\frac{\partial^2 S_{yy}}{\partial y^2}\right), \tag{1}$$

where $\bar{\zeta}$ is the slowly varying mean water surface, ρ is density, and g is acceleration due to gravity. Further S_{ij} is the radiation stress given by (2.14)[I]:

$$\frac{1}{\rho g}S_{ij}=\tfrac{1}{2}|A|^2\left\{\left(\frac{c_g}{c}-\frac{1}{2}\right)\delta_{ij}+\frac{c_g}{c}\frac{k_i k_j}{k^2}\right\}, \tag{2}$$

where δ_{ij} is the Kronecker delta and

$$\frac{k_i k_j}{k^2}=\begin{bmatrix}\cos^2\alpha & \tfrac{1}{2}\sin 2\alpha\\ \tfrac{1}{2}\sin 2\alpha & \sin^2\alpha\end{bmatrix}, \tag{3}$$

α being the local angle of incidence. A is a slowly varying complex amplitude describing the modulation of the short waves, and c_g and c are the group velocity and phase velocity of the short waves, respectively.

We only consider the case of two short-wave trains of amplitudes a and δa, $\delta \ll 1$ and slightly different angular frequencies for which the mean value is ω_s and the difference is ω.

As these modulated waves approach the shore, the break-point position changes in time and possibly part of the modulation persists after initial breaking has occurred. A detailed discussion in I of these phenomena led to the following expression for the modulated short-wave amplitude:

$$|A|^2=\begin{cases}\gamma_0^2 h^2(1+(1-\kappa)\,2\delta\cos 2\theta), & x\leqslant x_b(t)\\ a^2(1+2\delta\cos 2\theta), & x\geqslant x_b(t),\end{cases} \tag{4}$$

see (4.3)[I]. Here γ_0 is the ratio of the regular-wave breaker amplitude to breaker depth, $x_b(t)$ is the instantaneous break-point position, θ is defined below, and κ is a parameter close to unity introduced in I to model partial transmission of wave grouping into the surface zone. For $\kappa = 0$ the model reduces to one with a fixed break-point position and a full transmission of wave grouping. A more realistic value is $\kappa = 1$ which gives the special case where all the modulation of the incident groups is 'used up' in producing oscillations in the break-point position and no modulations penetrate to the surf zone. In I it was concluded that κ is probably around 1.1. This is close to unity and hence the canonical case of $\kappa = 1$ is used throughout the present paper.

We shall only consider a plane sloping beach $h = h_x x$ connected to a shelf $h = h_0$ outside the break point. Figure 1 (figure 3 in I) shows the bottom topography and a schematic representation of the primary waves in the two cases of $\kappa = 0$ and 1. The figure also defines region I as the surf zone, region II as the rest of the slope, and region III as the shelf. In the case of an oscillating break-point position a region B overlapping part of regions I and II is defined as the zone where initial breaking occurs.

Defining a modified time t' given by

$$\omega t' \equiv \omega t + K_y y \tag{5}$$

† The superscript I refers to an equation in Schäffer (1993).

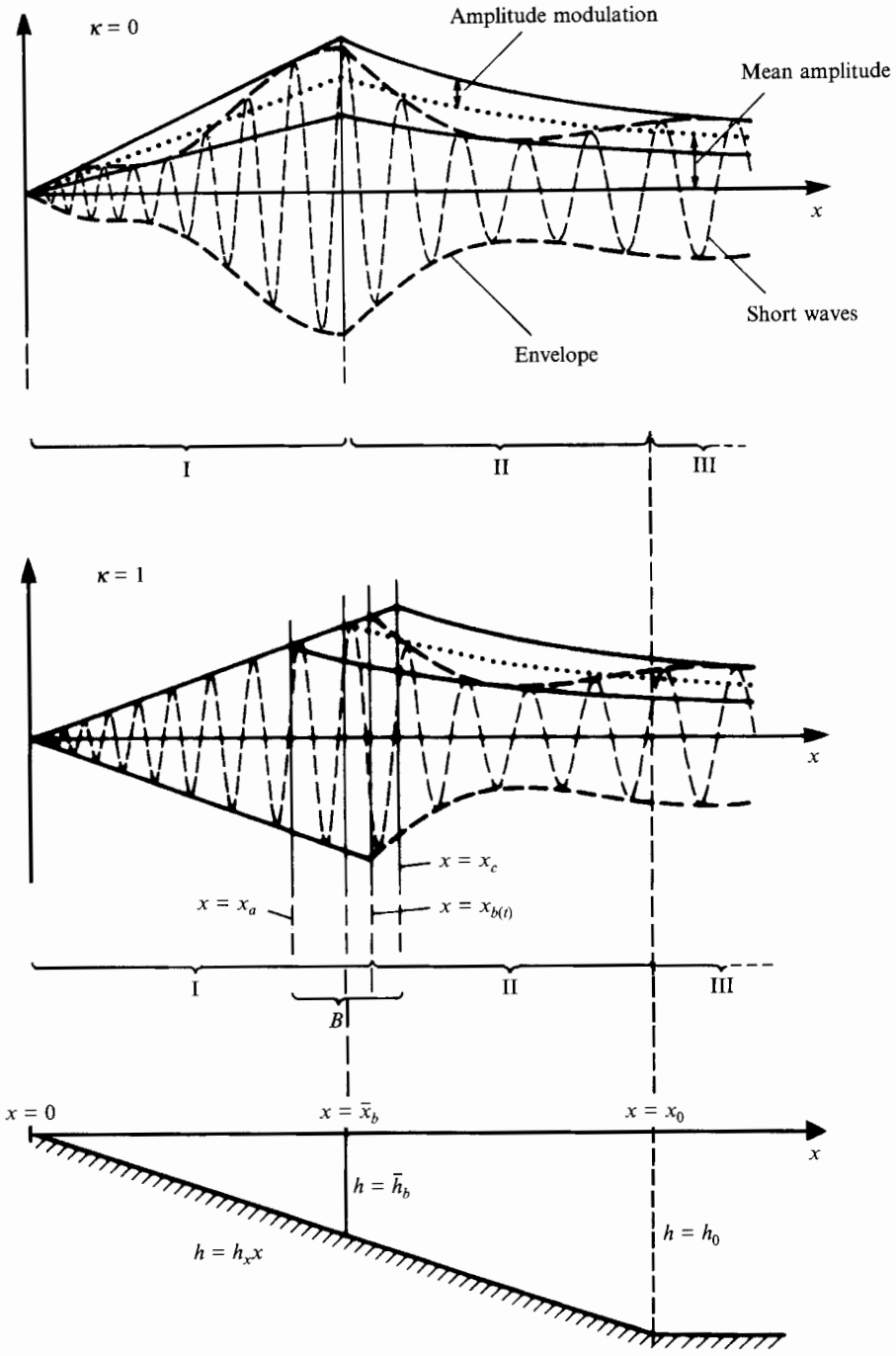

FIGURE 1. Sketch of bottom topography and two examples of short-wave modelling with associated definitions of the regions I, II, B, and III. From Schäffer (1993).

$(2.28)^{\mathrm{I}}$ and $(2.35)^{\mathrm{I}}$ yield

$$2\theta = \int_{\bar{x}_b}^{x} K_x \,\mathrm{d}x + \omega t'. \tag{6}$$

Here K_x and K_y are the components of the short-wave difference wavenumber, (2.22)[I] and (2.23)[I], which by (2.35)[I] may be written

$$K_x = \frac{\omega}{\omega_s}\frac{c_0}{c_{g0}}\left(k_x + \frac{k^2}{k_x}\left(\frac{c/c_g}{c_0/c_{g0}} - 1\right)\right), \tag{7}$$

$$K_y = \frac{\omega}{\omega_s}\frac{c_0}{c_{g0}}k_y, \tag{8}$$

where c_0 and c_{g0} are the phase and group velocity for the mean angular frequency ω_s on a reference depth h_0. Furthermore $(-k_x, -k_y)$ are the components of the mean wavenumber vector, where the minus is inferred to obtain positive values of k_x and k_y (see figure 2 in I). K_x and K_y were obtained from the kinematics of the two primary wave trains constituting the wave groups. Equivalent results were found by Mei & Benmoussa (1984) using the conservation equation of energy. Slight differences between the results are due to their use of a wavenumber perturbation while a frequency perturbation is used in the present approach.

The break point is found as the point where the two expressions for $|A|$ in (4) match. This results in an implicit expression for $x_b(t')$ which may be solved to get

$$x_b(t') = \frac{\bar{a}_b}{\gamma_0 h_x}(1 + \mu\kappa\delta\cos\omega t'), \tag{9}$$

see (2.46)[I]. Here the subscript b refers to the break point and an overbar denotes the time mean over a group period. The factor μ is close to unity, and it appears owing to the short-wave shoaling and refraction within the limits of the varying break-point position. The interested reader is referred to the derivation in I, see (2.38)[I].

With the shelf depth as reference, shoaling and refraction of the primary waves yields

$$a^2 = \frac{c_{gx,0}}{c_{gx}}a_0^2, \quad x \geqslant x_b(t), \tag{10}$$

where c_{gx} is the cross-shore component of the group velocity, see (2.30)[I].

Clearly the model described by (1)–(10) only applies to an idealized situation which is more likely to appear in a laboratory experiment than in nature. Furthermore, all expressions are given to the lowest order of accuracy and wave breaking is represented by the simple parametric formulation in (4). Altogether this makes the model more suitable for obtaining a basic understanding of the mechanisms behind the phenomena than for field applications.

3. Theoretical infragravity-wave solution

In this section we generalize the results of I (§§4.1 and 4.2) so as to account for an oblique incidence of the short-wave groups. The mathematical development in the region of initial short-wave breaking is different from but consistent with the two-dimensional model, which appears as a special case of the present findings.

Since the oblique short-wave incidence results in a radiation stress which has a variation in the longshore direction, the short-wave forcing will result in three-dimensional infragravity waves. However, for the one-dimensional topography considered this forcing is periodic alongshore and the longshore variation can be treated just as the periodic time-variation was treated in I.

3.1. *General solution*

Restricting ourselves to study only infragravity wave phenomena that are periodic in time as well as in the alongshore direction, we introduce the Fourier expansion of the elevation of mean water surface $\bar{\zeta}$:

$$\bar{\zeta} = \sum_{n=0}^{\infty} \frac{1}{2}(\xi_m \mathrm{e}^{\mathrm{i}n\omega t'} + *), \tag{11}$$

where $*$ denotes the complex conjugate of the preceding term. Here t' is time modified to include the alongshore periodic variation, see (5). In order to avoid getting three different expansions for the components of the radiation stress we define a tensor $s_{ij}(x)$ by

$$S_{ij}(x, t') \equiv s_{ij}(x)\,|A(x, t')|^2 \tag{12}$$

and expand only the part that has a variation with the modified time:

$$|A|^2 = \sum_{n=0}^{\infty} \frac{1}{2}(b_n \mathrm{e}^{\mathrm{i}n\omega t'} + *). \tag{13}$$

Now (1) transforms into the ordinary differential equations

$$\frac{\mathrm{d}}{\mathrm{d}x}\left(gh\frac{\mathrm{d}\xi_n}{\mathrm{d}x}\right) + ((n\omega)^2 - gh(nK_y)^2)\,\xi_n = ghq_n, \quad n = 0, 1, 2, \ldots, \tag{14}$$

where

$$q_n = \frac{-1}{\rho gh}\left(\frac{\mathrm{d}^2(b_n s_{xx})}{\mathrm{d}x^2} + 2\mathrm{i}nK_y\frac{\mathrm{d}(b_n s_{xy})}{\mathrm{d}x} - (nK_y)^2 b_n s_{yy}\right). \tag{15}$$

The case $n = 0$ determines the stationary set-down or set-up, and it will not be pursued further. For $n \geqslant 1$ (14) governs the infragravity-wave motion which we shall concentrate on in the following.

By the method of variation of parameters the solution to (14) may be expressed as

$$\xi_n = -\xi_n^{(1)}\left(-\alpha_n + \int_{x_l}^{x} \frac{\xi_n^{(2)} q_n}{W_n}\,\mathrm{d}x\right) + \xi_n^{(2)}\left(\beta_n + \int_{x_l}^{x} \frac{\xi_n^{(1)} q_n}{W_n}\,\mathrm{d}x\right), \quad n = 1, 2, 3, \ldots, \tag{16}$$

where $\xi_n^{(1)}$ and $\xi_n^{(2)}$ are linearly independent homogeneous solutions (free waves), W_n is their Wronskian, and α_n and β_n are arbitrary complex constants. Any lower limit of integration x_l in (16) can be chosen.

On the slope we have $h = h_x x$, and choosing a real representation the free-wave solutions (homogeneous solutions) to (14) are given by the confluent hypergeometric functions of the first and second kind† multiplied by an exponential function ($n = 1, 2, 3, \ldots$):

$$\xi_n^{(1)} = \mathrm{e}^{-nz'/2} M(a, 1, nz'), \quad \xi_n^{(2)} = \mathrm{e}^{-nz'/2} U_m(a, 1, nz'), \tag{17}$$

where

$$z' \equiv 2K_y x, \quad a = -\frac{1}{2}\left(\frac{n\omega^2}{gh_x K_y} - 1\right). \tag{18}$$

The parameter a is non-dimensional and should not be confused with the dimensional unmodulated primary-wave amplitude in (10).

Note that for $-a = 0, 1, 2, \ldots, M$ $(a, 1, nz')$ reduces to the *Laguerre polynomial* of

† Usually the latter is denoted $U(a, 1, z')$. The subscript m refers to modifications necessary in order to obtain a solution that is defined even when a is a negative integer or zero, see the Appendix.

order $-a$, $L_{-a}(nz')$, and $\xi_n^{(1)}$ reduces to the shallow-water edge-wave solution, see Eckart (1951), or Schäffer & Jonsson (1992). The Wronskian of the functions in (17)† with respect to x is (due to our definition of z' in (18))

$$W_n = \frac{1}{nz'}\frac{\mathrm{d}}{\mathrm{d}x}(nz') = \frac{1}{x} \tag{19}$$

and we get

$$\frac{q_n}{W_n} = -\frac{1}{\rho g h_x}\left(\frac{\mathrm{d}^2(b_n s_{xx})}{\mathrm{d}x^2} + 2\mathrm{i}nK_y\frac{\mathrm{d}(b_n s_{xy})}{\mathrm{d}x} - (nK_y)^2 b_n s_{yy}\right), \quad n = 1,2,3,\ldots, \tag{20}$$

On the shelf ($h = h_0$) the solution to (14) is easily verified to be (for $\lambda \neq 0$)

$$\xi_n^{(\mathrm{III})} = \alpha_n^{(\mathrm{III})}\exp(n\lambda^{\frac{1}{2}}K_y x) + \beta_n^{(\mathrm{III})}\exp(-n\lambda^{\frac{1}{2}}K_y x) + \begin{cases} \dfrac{b_1 s_{xx}^{(\mathrm{III})}\cos^2\alpha_0 + 2s_{xy}^{(\mathrm{III})}\sin\alpha_0\cos\alpha_0 + s_{yy}^{(\mathrm{III})}\sin^2\alpha_0}{\rho\, gh_0 - c_{g0}^2}, & n = 1 \\ 0, & n = 2,3,4,\ldots, \end{cases} \tag{21}$$

where

$$\lambda \equiv 1 - \omega^2/(gh_0 K_y^2) \tag{22}$$

and α_0 is the angle of incidence on the shelf. The sign of λ determines whether the free-wave solutions are progressive or standing waves in the cross-shore direction. In (21) the particular solution (last term) is the bound, long wave found by Longuet-Higgins & Stewart (1962, 1964), now expressed in a coordinate system rotated an angle α_0 relative to the direction of group propagation.

The assumption of wave groups made up from only two wave components reduces (13) to

$$(|A|^2)^{(J)} = b_0^{(J)} + \tfrac{1}{2}(b_1^{(J)}\mathrm{e}^{\mathrm{i}\omega t'} + *), \quad J = \mathrm{I}, \mathrm{II}, \mathrm{III}, \tag{23}$$

where J refers to three regions: Region I is the surf zone, region II is the rest of the slope, and region III is the shelf, see figure 1.

Further b_0 and b_1 are given by

$$b_0 = \begin{cases} \gamma_0^2 h^2, & x \leqslant x_b(t') \\ a^2, & x \geqslant x_b(t') \end{cases} \tag{24}$$

and

$$b_1 = \begin{cases} \gamma_0^2 h^2(1-\kappa)\,2\delta\exp\left(\mathrm{i}\int_{\bar{x}_b}^{x} K_x\,\mathrm{d}x\right), & x \leqslant x_b(t') \\ a^2 2\delta\exp\left(\mathrm{i}\int_{\bar{x}_b}^{x} K_x\,\mathrm{d}x\right), & x \geqslant x_b(t'). \end{cases} \tag{25}$$

3.2. *The effect of oscillations of the break-point position*

The implicit time-dependence hidden in the variable break-point position is essential. The mathematical consequence of this time variation is that within the spatial limits of the break-point position, which we shall refer to as region B, (24) and (25) are *not* the Fourier coefficients of $|A|^2$. However, these can be found along the lines of I (§4.2.2) using the modified time t' in place of t, see Schäffer (1990) for details.

† According to the differential equation (14) the Wronskian should be $\propto 1/x$ (for $h \propto x$) and numerical computations of (17) and their derivatives showed that the factor of proportionality was unity (as used in (19)) for our choice of U_m (based on $d_0 = 2$, see the Appendix).

Returning to the expression for the elevation (16) we can write a particular solution in region B as

$$\xi_n^{(\mathrm{B})} = \xi_n^{(1)} \int_{x_a}^{x} \frac{\mathrm{d}\xi_n^{(2)}}{\mathrm{d}x} Q_n \,\mathrm{d}x - \xi_n^{(2)} \int_{x_a}^{x} \frac{\mathrm{d}\xi_n^{(1)}}{\mathrm{d}x} Q_n \,\mathrm{d}x, \tag{26}$$

where

$$Q_n \equiv \int_{x_a}^{x} \frac{q_n}{W_n} \mathrm{d}x \tag{27}$$

and the shoreward limit of the variable break-point position (see figure 1) is taken as the lower limit of integration. Here integration by parts was applied and $n = 1, 2, 3, \ldots$ is understood. Now all variables in (26) except q_n are slowly varying in region B, and within errors of $O(\delta)$ (giving errors on $\xi_n^{(\mathrm{B})}$ of $O(\delta^2)$ which we neglect) they can be approximated by their values at the mean break-point position. This way (26) yields

$$\begin{aligned} \xi_n^{(\mathrm{B})} &= \left(\xi_n^{(1)} \frac{\mathrm{d}\xi_n^{(2)}}{\mathrm{d}x} - \xi_n^{(2)} \frac{\mathrm{d}\xi_n^{(1)}}{\mathrm{d}x} \right) \int_{x_a}^{x} Q_n \,\mathrm{d}x \\ &= W_n \int_{x_a}^{x} Q_n \,\mathrm{d}x \\ &= \int_{x_a}^{x} \int_{x_a}^{x} q_n \,\mathrm{d}x \,\mathrm{d}x. \end{aligned} \tag{28}$$

From (15) we have (to the sufficient accuracy, i.e. neglecting terms of $O(\delta)$)

$$\int_{x_a}^{x} q_n \,\mathrm{d}x = -\frac{1}{\rho g \bar{h}_b} \left(\left[\frac{\mathrm{d}(b_n^{(\mathrm{B})} s_{xx})}{\mathrm{d}x} \right]_{x_a}^{x} + [2inK_y b_n^{(\mathrm{B})} s_{xy}]_{x_a}^{x} - \int_{x_a}^{x} (nK_y)^2 b_n^{(\mathrm{B})} s_{yy} \,\mathrm{d}x \right), \tag{29}$$

where $\bar{h}_b$ is the depth at the mean break-point position. Now $b_n^{(\mathrm{B})}$ is $O(\delta)$ and it follows that the last two terms are $O(\delta)$ and $O(\delta^2)$, respectively. Further $\mathrm{d}b_n^{(\mathrm{B})}/\mathrm{d}x$ is $O(\delta^0)$ except at the endpoint x_a and we have

$$\begin{aligned} -\frac{1}{\rho g \bar{h}_b} \left[\frac{\mathrm{d}(b_{n\, s_{xx}}^{(\mathrm{B})})}{\mathrm{d}x} \right]_{x_a}^{x} &= -\frac{1}{\rho g \bar{h}_b} \frac{\mathrm{d}(b_n^{(\mathrm{B})} s_{xx})}{\mathrm{d}x} + O(\delta) \\ &= O(\delta^0). \end{aligned} \tag{30}$$

This means that we only need to retain the contribution from the upper variable endpoint of the first term in (29), and we get

$$\int_{x_a}^{x} q_n \,\mathrm{d}x = -\frac{1}{\rho g \bar{h}_b} \frac{\mathrm{d}(b_n^{(\mathrm{B})} s_{xx})}{\mathrm{d}x}, \tag{31}$$

neglecting terms of $O(\delta)$. Using this in (28) yields

$$\xi_n^{(\mathrm{B})} = -\frac{1}{\rho g \bar{h}_b} [b_n^{(\mathrm{B})} s_{xx}]_{x_a}^{x} = -\frac{1}{\rho g \bar{h}_b} s_{xx} [b_n^{(\mathrm{B})}]_{x_a}^{x}, \tag{32}$$

neglecting terms of $O(\delta^2)$. In terms of $b_0^{(1)}$ at $x = \bar{x}_b$ the 'jump' in the elevation over region B can finally be written

$$\left.\begin{aligned} [\xi_1]_-^+ &= -\frac{2\kappa\delta}{\rho g \bar{h}_b}[s_{xx} b_0^{(1)}], \\ [\xi_n]_-^+ &= 0, \quad n = 2, 3, 4, \ldots, \end{aligned}\right\} \quad x = \bar{x}_b \tag{33}$$

where we have replaced the endpoints of region B with $\bar{x}_b$, consistent with earlier approximations.

The 'jump' condition in the formulation of (33) is consistent with the one obtained by a different mathematical development in the two-dimensional case (cf. (4.43)[I]) although it involves neither μ nor the derivatives of the radiation stress. The two forms are seen to be equivalent if

$$\mu\left[\frac{\mathrm{d}(b_0 s_{xx})}{\mathrm{d}x}\right]_-^+ = -\left[\frac{2}{x} b_0 s_{xx}\right], \quad x = \bar{x}_b, \tag{34}$$

which to the leading order in δ may be written

$$\mu\left[\frac{\mathrm{d}b_0}{\mathrm{d}x}\right]_-^+ = -\frac{2b_0}{x}, \quad x = \bar{x}_b \tag{35}$$

or

$$\mu\left[2a\frac{\mathrm{d}a}{\mathrm{d}x} - 2\gamma_0^2 h h_x\right] = -\left[\frac{2a^2}{x}\right], \quad x = \bar{x}_b, \tag{36}$$

and since $a = \gamma_0 h$ at $x = \bar{x}_b$ this may be written as

$$\mu\left[-\frac{x}{a}\frac{\mathrm{d}a}{\mathrm{d}x} + 1\right] = 1, \quad x = \bar{x}_b \tag{37}$$

which is satisfied, since by definition $\mu \equiv 1/(1+\nu)$ where $\nu \equiv -[(x/a)(\mathrm{d}a/\mathrm{d}x)]_{x=\bar{x}_b}$, see (2.38)[I], q.e.d.

Were now turn to the gradient of the surface elevation to investigate whether the 'kink' in the elevation over region B is also the same as in the two-dimensional case. Along the lines of derivations in I (see Schäffer 1990 for details) this leads us to the expressions

$$\left.\begin{aligned} \left[\frac{\mathrm{d}\xi_1}{\mathrm{d}x}\right]_-^+ &= -\frac{1}{\rho g h_x x}\left[\frac{\mathrm{d}(b_1 s_{xx})}{\mathrm{d}x} + 2\mathrm{i}K_y s_{xy} b_1\right]_-^+, \\ \left[\frac{\mathrm{d}\xi_n}{\mathrm{d}x}\right]_-^+ &= 0, \quad n = 2, 3, 4, \ldots, \end{aligned}\right\} \quad x = \bar{x}_b, \tag{38}$$

where b_1 is now formally evaluated in the limits of regions I and II as valid for a vanishing extent of region B.

As in the two-dimensional case there *is* a kink in the elevation of the fundamental, but no kink in the higher harmonics. Since the forcing outside region B is also zero for the higher harmonics we can conclude that $\xi_n \equiv 0$ for $n = 2, 3, 4, \ldots$ to the lowest order of approximation in δ. Comparing this result with the matching conditions of §2.1.3 in I, we see that (38) satisfies (2.13)[I].

The important conclusion of this subsection is that we can incorporate the effect of oscillations of the break-point position in the overall solution for the surface elevation

by simply ignoring the presence of region B and replacing the continuity condition (2.12)[I] by the discontinuity condition (33) applying also the kink condition (38). This is analogous to the two-dimensional case of normal short-wave incidence.

Physically the importance of time-varying break point is due to oscillations in the starting point of the set-up, affecting the whole surf zone and not only region B. Had $b_n^{(B)}$ only been a weighted mean of $b_n^{(I)}$ and $b_n^{(II)}$, it would have been of no significance.

3.3. *Determination of integration constants*

As in the case of normal incidence there are two complex constants in three regions to be determined, and we have two boundary conditions and four matching conditions providing the necessary six complex equations.

For $\lambda < 0$ the homogeneous solutions in region III (see (21)) are progressive free long waves, and the seaward boundary condition (cf. §2.1.2 in I) is that of no incoming free long waves, which requires

$$\alpha_1^{(III)} = 0. \tag{39}$$

On the other hand, for $\lambda > 0$ these solutions are standing free long waves (in the offshore direction), and we only retain the evanescent mode. This also leads to (39). For $\lambda = 0$ the homogeneous solution to (14) in region III can be written as $\alpha_1^{(III)}(h_x x) + \beta_1^{(III)}$, and its represents free long waves travelling parallel to the shoreline. As for $\lambda > 0$ the component with seaward growth must be ruled out, and it follows that (39) can be used for any λ. Furthermore, applying (39) to (21), the case of $\lambda = 0$ need no longer be excluded from (21).

In region I we take $x_l = 0$ as the lower limit of integration in (16) by which the particular part of the solution vanishes at the shoreline. Now the limited-amplitude reflection condition is

$$\hat{\beta}_1^{(I)} = 0 \tag{40}$$

since $\xi_1^{(1)}$ is regular at the shoreline, while $\xi_1^{(2)}$ is singular there, cf. (17).

The matching conditions at $\bar{x}_b$ are given by (33) and (38). At x_0 where the slope meets the shelf, conditions of continuity in surface elevation and depth-integrated velocity are applied, see (2.12)[I] and (2.13)[I].

3.4. *Horizontal particle velocity and mean energy flux*

As for the case of normally incident wave groups the Fourier expansion of the linearized horizontal long-wave particle-velocity components

$$U_i = \sum_{n=0}^{\infty} \frac{1}{2}(U_{n,i} e^{in\omega t'} + *), \quad i = x, y \tag{41}$$

together with the equation of conservation of momentum yields (for $n \neq 0$†)

$$U_{n,i} = \frac{i}{n\omega}\left(g\frac{d\xi_n}{dx_i} + \frac{1}{\rho h}\frac{d(b_n s_{ij})}{dx_j}\right). \tag{42}$$

Now $U_n \equiv 0$ for $n = 2, 3, 4, \ldots$, since for these n-values both ξ_n and b_n vanish and thus the time-dependent horizontal velocity is described by $U_{1,i}$ alone.

The expression for the mean energy flux W_i of the long-wave motion is similar to the

† Note that $n = 0$ corresponds to the steady currents. However, the longshore current $U_{0,y}$ cannot be determined by conservation of momentum without adding a frictional term, since otherwise there is nothing to balance the shore-normal gradient of the S_{xy}-term.

one for the cross-shore case as well, see (4.50)[I]. We get, excluding the energy flux of the steady current,

$$\left.\begin{aligned} W_i &= \frac{1}{T}\int_0^T \rho g h \bar{\zeta}(U_i - U_{0,i})\,\mathrm{d}t \\ &= \frac{1}{2}\rho g h \,\mathrm{Re}\{U_{1,i}\,\xi_1^*\} \end{aligned}\right\} \tag{43}$$

(see (4.50)[I] for details), where $*$ as before denotes the complex conjugate of the actual term when used as a superscript.

3.5. *Important parameters*

The following non-dimensional forms (marked with $\hat{}$) are chosen:

$$\hat{\xi}_1 = \frac{\xi_1}{\delta a_0}, \quad \hat{U}_{1,i} = \frac{U_{1,i}}{\delta \omega_s a_0}, \quad \hat{W}_i = \frac{W_i}{\delta^2 W_{s0}}, \tag{44}$$

where W_{s0} is the short-wave energy flux before breaking.

With these non-dimensional forms the solution can be reduced to depend on the following six parameters:

$$h_x \omega_s/\omega, \quad \hat{h}_0, \quad \hat{a}_0, \quad \kappa, \quad \gamma_0, \quad \alpha_0. \tag{45}$$

Here $h_x \omega_s/\omega$ is the small bottom slope scaled with the small ratio of the timescale of the primary waves and the timescale of the infragravity waves, $\hat{h}_0$ and $\hat{a}_0$ are the non-dimensional depth and unmodulated primary-wave amplitude, respectively, both at the shelf and both scaled by $k_\infty = \omega_s^2/g$, κ and γ_0 are the parameters used in the modelling of primary-wave breaking, and α_0 is the common angle of incidence over the shelf for the two short-wave trains constituting the groups.

Although we generally take (45) as the input for the model, three other parameters are very important for the solution. These are $-a$, z_0', and λ, and they are all functions of the parameters in (45) in the sense that their values can be found without solving the infragravity-wave equations. The significance of the parameter $-a$ can be assessed by noting that, in the absence of the shelf, $-a = 0, 1, 2, \ldots$ would identify an edge-wave mode. The parameter z_0' is the dimensionless distance from the coastline to the shelf.

From (18) for $n = 1$ we get

$$-a = \frac{1}{2}\left(\frac{1}{(h_x \omega_s/\omega)\hat{k}_0(c_0/c_{g0})\sin\alpha_0} - 1\right) \tag{46}$$

and

$$z_0' = \frac{2\hat{h}_0 \hat{k}_0 (c_0/c_{g0})\sin\alpha_0}{h_x \omega_s/\omega} \tag{47}$$

also using (8). From (22) we get

$$\lambda = 1 - \frac{1}{\hat{h}_0(\hat{k}_0(c_0/c_{g0})\sin\alpha_0)^2}, \tag{48}$$

the sign of which determines whether the long-wave modes are trapped or leaky. Only for the trapped modes ($\lambda > 0$) is resonant-wave forcing possible. These three parameters are related by

$$z_0' = \frac{2(1-2a)}{1-\lambda}. \tag{49}$$

The angle of incidence corresponding to the turning point $\lambda = 0$ shall be denoted α_{cr}. This angle is solely a function of $\hat{h}_0$, and from (48) we get

$$\sin\alpha_{cr} = \frac{1}{\hat{h}_0^{\frac{1}{2}}\hat{k}_0\, c_0/c_{g0}}. \tag{50}$$

Only in the limit where the shelf depth corresponds to shallow water for the primary waves do we have $\sin\alpha_{cr} = 1$ and no trapping is possible.

In terms of α_0 and α_{cr} we can write λ as

$$\lambda = 1 - \left(\frac{\sin\alpha_{cr}}{\sin\alpha_0}\right)^2. \tag{51}$$

Finally it is instructive to introduce a non-dimensional caustic depth $\hat{h}_c$ defined as

$$\hat{h}_c \equiv \left(\frac{1}{\hat{k}_0\,(c_0/c_{g0})\sin\alpha_0}\right)^2 \tag{52}$$

which appears from (48) with $\lambda = 0$. The dimensional form of $\hat{h}_c$ is $h_c = \omega^2/(gK_y^2)$ (see (22)) and it comes from regarding the long-wave from a geometrical optics point of view, see Schäffer & Jonsson (1992). For $\hat{h}_0 > \hat{h}_c$ a caustic exists, and we have trapped modes, while for $\hat{h}_0 < \hat{h}_c$ there is no trapping, and $\hat{h}_c$ represents the non-existent depth at which the caustic *would* have been for the given long-wave frequency and long-wave alongshore wavenumber in the absence of the shelf. In terms of $\hat{h}_0$ and $\hat{h}_c$, λ takes the form

$$\lambda = 1 - \hat{h}_c/\hat{h}_0. \tag{53}$$

Note that for $\lambda < 0$, $-\arctan(1-(-\lambda)^{\frac{1}{2}})$ gives the angle of reflection for the seaward emitted free long wave, cf. the phase in the second term of the right-hand side of (21) for $n = 1$.

For normally incident short waves a 'reflection coefficient' R was defined as the ratio between the free long wave propagating seawards over the shelf (region III) and the incident bound long wave, see (4.53)[I].

When trapping of the long waves occurs (i.e. $\lambda > 0$) there is no emission of progressive free long waves in region III, and one could argue that the reflection coefficient should then be zero. However, we might as well use the information provided by the following definition of R:

$$R = \frac{|\beta_1^{(\mathrm{III})}\exp(-\lambda^{\frac{1}{2}}K_y x)|}{\left|\dfrac{\frac{b_1}{\rho}s_{xx}^{(\mathrm{III})}\cos^2\alpha_0 + 2s_{xy}^{(\mathrm{III})}\sin\alpha_0\cos\alpha_0 + s_{yy}^{(\mathrm{III})}\sin^2\alpha_0}{gh_0 - c_{g0}^2}\right|}. \tag{54}$$

For leaky modes (i.e. $\lambda < 0$, cf. (22)) this definition is consistent with the definition (4.53)[I], and it gives the ratio between the respective amplitudes of the free long waves propagating seawards in region III and the incoming bound long wave. For trapped modes R becomes the ratio between the respective amplitudes of the free evanescent mode measured at $\hat{x} = \hat{x}_0$ and the incoming bound long wave.

Note that for trapped modes R is very small for large $\hat{h}_0$ as opposed to the case of leaky modes, cf. §4.2.5 in I.

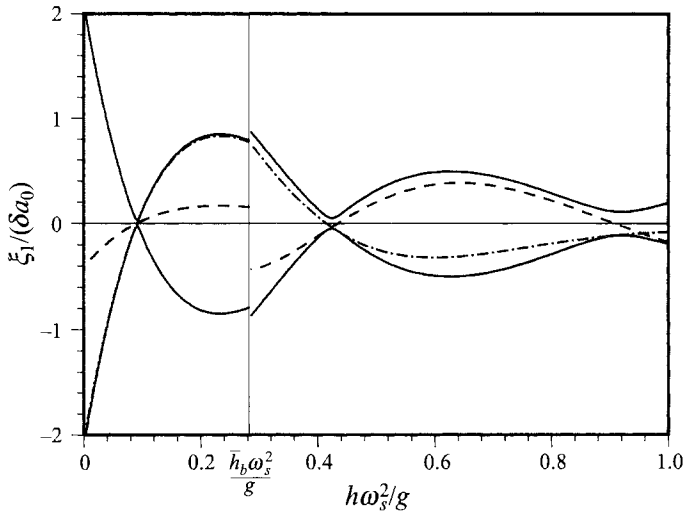

FIGURE 2. Dimensionless infragravity wave: ——, envelope $\pm|\hat{\xi}_1|$, and elevations – – –, $\mathrm{Re}\{\hat{\xi}_1\}$ at $t = 0$, and –·–·–, $\mathrm{Im}\{\hat{\xi}_1\}$ at $t = T/4$, versus $\hat{h}$ for the input parameters $h_x\omega_s/\omega = 0.25$, $\hat{h}_0 = 1$, $\hat{a}_0 = 0.1$, $\kappa = 1$, $\gamma_0 = 0.4$, and $\alpha_0 = 15°$, which yield $R = 1.8$.

4. Sample results for the infragravity wave

4.1. *Surface elevation*

As in the shore-normal case the solution (16) for ξ_1 was integrated numerically, and the integration constants were found by numerical solution of the six linear equations. The parameters used as input for the model are given in (45), and in the example of figure 1 we have used $\alpha_0 = 15°$, $h_x\omega_s/\omega = 0.25$, $\hat{h}_0 = 1$, $\hat{a}_0 = 0.1$, $\kappa = 1$, and $\gamma_0 = 0.4$. The value of $\kappa = 1$, specifies that all wave grouping is used in producing oscillations in the break-point position so that no modulations are transmitted into the surf zone. Figure 2 shows the envelope of the infragravity waves (not to be confused with the envelope of the short waves), which is given by $\pm|\hat{\xi}_1|$. Furthermore, $\mathrm{Re}\{\hat{\xi}_1\}$ and $\mathrm{Im}\{\hat{\xi}_1\}$ are shown. These correspond to the surface elevation at times $t = 0$ and $t = -T/4$, respectively, where $T = 2\pi/\omega$ is the infragravity-wave period, which is identical with the group period of the short waves. The figures shows the whole sloping region but not the shelf (this also applies to figures 3–7). Note the jump in the elevation at the mean break-point position. This represents the significant forcing that takes place within the limits of the variable break-point position. Figure 2 is almost identical with the equivalent solution for normal incidence. This indicates that the oblique incidence has virtually no effect, at least as long as α_0 is small. For $\hat{h}_0 = 1$ the critical angle of incidence is $\alpha_{cr} = 36.86°$, i.e. no trapping for $\alpha_0 = 15°$. Leaving all other input parameters unchanged ($h_x\omega_s/\omega = 0.25$, $\hat{h}_0 = 1$, $\hat{a}_0 = 0.1$, $\kappa = 1$, $\gamma_0 = 0.4$), figure 3(*a*, *b*) shows the solution for $\alpha_0 = 30°$ and $\alpha_0 = 45°$, respectively. Comparing figure 3(a) ($\alpha_0 = 30°$) with figure 2 ($\alpha_0 = 15°$) we see that the effect of the larger angle of incidence is surprisingly small. Even for $\alpha_0 = 45°$ (figure 3*b*), for which we have long-wave trapping (since $\alpha_0 > \alpha_{cr}$), the solution appears much the same, at least inside the surf zone. Outside the surface zone though, there is a qualitative change in that the 'almost-node' in figures 2 and 3(*a*) disintegrates as expected. In figure 3(*b*) the caustic depth is $\hat{h}_c = 0.72$.

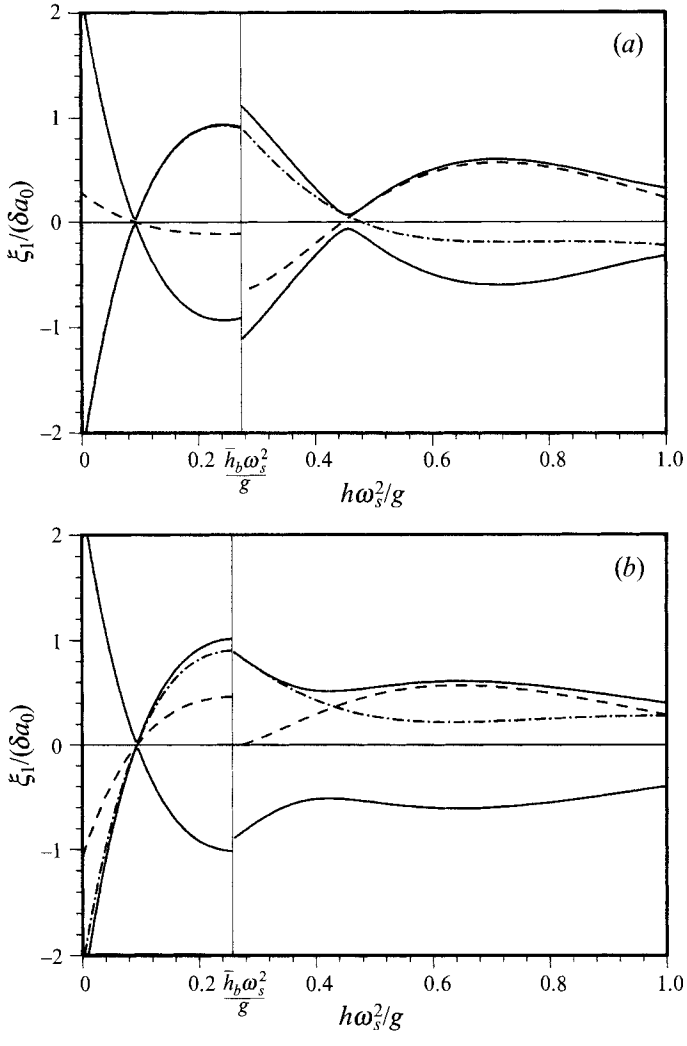

FIGURE 3. As figure 2 but for (*a*) $\alpha_0 = 30°$, which yields $R = 2.9$, and (*b*) $\alpha_0 = 45°$, which yields $R = 1.7$.

4.2. *Mean energy flux and horizontal particle velocity*

Figure 4 shows the components of the mean long-wave energy flux $\hat{W}_i$ versus $\hat{h}$ for the solution shown in figure 2 ($\alpha_0 = 15°$). The cross-shore component closely resembles that of normal incidence (figure 4.12*b* in Schäffer 1990), although no direct quantitative comparison can be made because of the different choice of reference depth. The vanishing cross-shore energy flux in the surf zone is a consequence of using $\kappa = 1$, which prohibits primary-wave modulations and thereby infragravity-wave forcing in the surface zone. Thus in the surface zone the solution represents a standing wave in the cross-shore direction. As for the corresponding surface elevation the jump in the energy flux is a consequence of the forcing mechanisms due to the oscillations in the break-point position. The longshore component is negative almost everywhere, indicating a flux of energy following the short waves. Even for this rather small angle of incidence the energy flux is of the same order of magnitude in the two directions.

Figure 5(*a*, *b*) shows $\hat{W}_i$ corresponding to the elevations shown in figure 4(*a*, *b*), i.e.

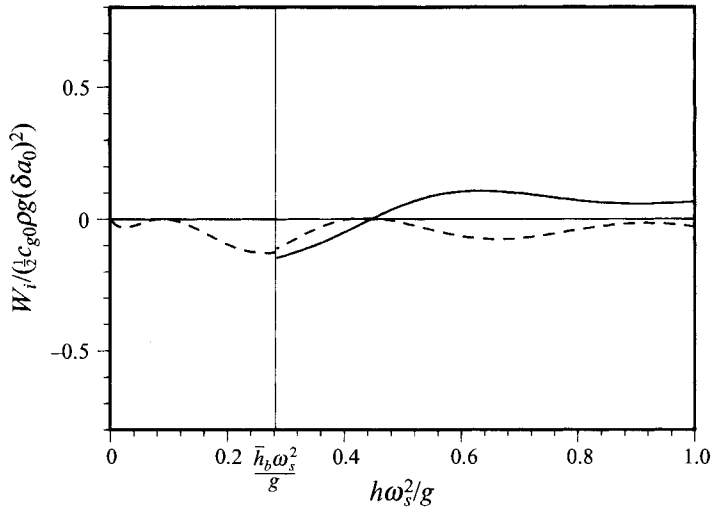

FIGURE 4. Mean infragravity-wave energy-flux components: ——, $\hat{W}_x$ and – – –, $\hat{W}_y$, versus $\hat{h}$ for the input parameters $h_x\omega_s/\omega = 0.25$, $\hat{h}_0 = 1$, $\hat{a}_0 = 0.1$, $\kappa = 1$, $\gamma_0 = 0.4$, and $\alpha_0 = 15°$.

for $\alpha_0 = 30°$ and 45°, respectively. The leaky-mode case of $\alpha_0 = 30°$ (figure 5*a*) appears somewhat the same as for $\alpha_0 = 15°$ (figure 4), although the seaward emission of energy is about twice as much for the larger α_0-value. The longshore energy flux is approximately tripled when changing from $\alpha_0 = 15°$ to 30°. For $\alpha_0 = 45°$ (figure 5*b*) $\hat{W}_x$ is negative at $\hat{h} = \hat{h}_0$ indicating a shoreward flux of energy. This is in accordance with the fact that in the trapped-mode case there is no seaward emission of free long waves, while the incident bound long wave still represents a shoreward energy flux.

Figure 6 shows the amplitude of the components of the non-dimensional horizontal particle velocity $|\hat{U}_{1,i}| = |U_{1,i}|/(\delta a_\infty \omega_s)$ for the infragravity wave shown in figure 2. The cross-shore component resembles that of the normal-incidence case (figure 11 in I). The longshore component is rather small.

Corresponding to the elevations in figure 3, figure 7(*a*, *b*) shows $\hat{U}_{1,i}$ for $\alpha_0 = 30°$ and 45°, respectively. The cross-shore component is still dominant inside the surface zone, while at $h_x\hat{x} = \hat{h}_0$, $\hat{U}_{1,y}$ approximately equals $\hat{U}_{1,x}$ for $\alpha_0 = 30°$, and for $\alpha_0 = 45°$ the longshore component takes the lead.

4.3. *The influence of varying input parameters*

In this subsection we analyse the effect of different input parameters on the solution as a whole. Important quantities describing the infragravity wave are the reflection coefficient R (note the special definition (54) of R), the infragravity-wave amplitude at the shoreline $|\xi_1(0)|/(\delta a_0)$, and the amplitude of the free long wave $|\xi_f|/(\delta a_0)$ measured at the edge of the shelf zone ($h_x\hat{x} = \hat{h}_0$). The variation of these quantities is now given for varying $h_x\omega_s/\omega$ and α_0, respectively.

For $0.1 \leqslant h_x\omega_s/\omega \leqslant 1$ the infragravity-wave solution was found using $\hat{h}_0 = 1$, $\hat{a}_0 = 0.1$, $\kappa = 1$, $\gamma_0 = 0.4$, and $\alpha_0 = 30°$. The resulting curves for R, $|\xi_1(0)|/(\delta a_0)$, and $|\xi_f|/(\delta a_0)$ can be represented in many ways, and figure 8(*a*, *b*) shows two of them. For comparison with figure 13(*b*) in I, figure 8(*a*) shows the results as a function of $\chi \equiv (h_x\omega_s/\omega)^{-2}\hat{\bar{h}}_b$, where $\hat{\bar{h}}_b = 0.273$ for the given values of α_0 and $\hat{a}_0$. In addition to the results from the infragravity-wave model, the parameter $h_x\omega_s/\omega$ is also shown. Figure 8(*a*) is very similar to figure 13(*b*) in I for which the input parameters were the same except for the angle of incidence and the use of reference depth. Note that this gives

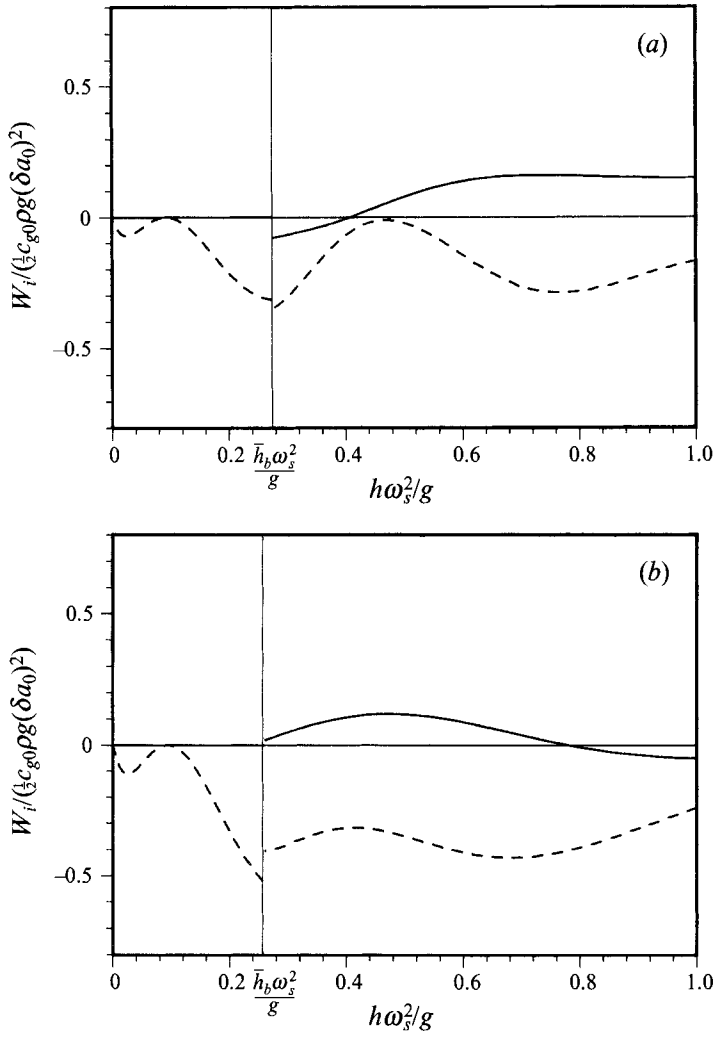

FIGURE 5. As figure 4 but for (*a*) $\alpha_0 = 30°$, and (*b*) $\alpha_0 = 45°$.

a slight difference in χ through $\hat{\bar{h}}_b$, and the figures are not quantitatively comparable. The increasing trend in R with decreasing $h_x\omega_s/\omega$ is a consequence of the smaller slope allowing for more time (or distance) to build-up incident low-frequency energy than the steeper slope as discussed in connection with figure 8 in I.

The oscillations in R can be explained as a result of a change in the phase difference between two essentially-free long waves. Both of these waves are generated in the region of initial breaking, but one is subject to direct seaward emission while the other is emitted after reflection from the shoreline. The parameter χ introduced by Symonds *et al.* (1982) is a measure of this relative phase, see Schäffer (1990) for a detailed discussion. Figure 8(*a*) also exhibits increasing infragravity-wave activity (see for example $|\xi_1(0)|/(\delta a_0)$) with increasing frequency, while field observations typically show the opposite trend. However, there is no contradiction, since for natural waves the concentration of primary-wave energy close to the peak frequency emphasizes the low-frequency forcing and hence the low-frequency infragravity-wave response. Figure 8(*b*) shows the same results as figure 8(*a*) but now as a function of $-a$, (46). This parameter is relevant when the short-wave incidence is oblique because special values of $-a$

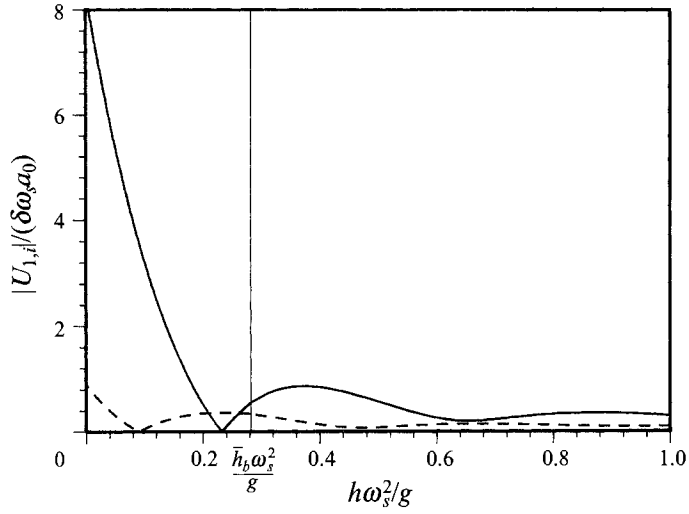

FIGURE 6. Amplitude of horizontal infragravity-wave particle-velocity components: ——, $\hat{U}_{1,x}$ and – – –, $\hat{U}_{1,y}$, versus $\hat{h}$ for the input parameters $h_x\omega_s/\omega = 0.25$, $\hat{h}_0 = 1$, $\hat{a}_0 = 0.1$, $\kappa = 1$, $\gamma_0 = 0.4$, and $\alpha_0 = 15°$.

satisfy the dispersion relation for free edge waves resulting in resonant edge-wave excitation. As mentioned above, the critical angle of incidence is $\alpha_{cr} = 36.86°$ for $\hat{h}_0 = 1$. This means that $\alpha_0 = 30°$ is really not very far from giving trapped modes. On the other hand the (non-existent) caustic depth is $\hat{h}_c = 1.44$ which compared with $\hat{h}_0 = 1$ gives the impression that trapping is not very close. A third measure of how far we are from getting trapped modes is the value of λ, which for the given $\hat{h}_0$ and α_0 is $\lambda = -0.44$.

We now increase the angle of incidence to $\alpha_0 = 35°$, which is very close to $\alpha_{cr} = 36.86°$. This yields $\hat{h}_c = 1.09$ and $\lambda = -0.094$, and the results are shown in figure 9(*a*) (again for $\hat{h}_0 = 1$, $\hat{a}_0 = 0.1$, $\kappa = 1$, and $\gamma_0 = 0.4$). Now marked peaks appear in R, $|\xi_1(0)|/(\delta a_0)$, and $|\xi_f|/(\delta a_0)$ for $-\alpha$ close to integer values. This is because we get close to the edge-wave dispersion curves, as will be shown below, and this near-resonance now dominates the importance of the relative phase mentioned above.

Increasing the angle of incidence to $\alpha_0 = 45°$ means that $\alpha_{cr} = 36.86°$ is well exceeded. Now $\hat{h}_c = 0.72$ and $\lambda = 0.280$, and the results are shown in figure 9(*b*) (again for $\hat{h}_0 = 1$, $\hat{a}_0 = 0.1$, $\kappa = 1$, and $\gamma_0 = 0.4$). The marked peaks have now turned into genuine singularities corresponding to resonant excitation of free edge waves. The fact that some of the peaks appear finite is only a consequence of the finite resolution of the abcissa.

Bowen & Guza (1978) conducted laboratory experiments on the forcing of (primarily mode 1) edge waves, and figure 9(*b*) is in qualitative agreement with their measurements (their figure 9). However, a number of differences between their experiments and the present model prohibits a quantitative comparison. The most important of these differences is the limited longshore extent of their experimental set-up, which prevents the development of steady-state infragravity waves, thus giving long-wave amplitudes which are an order of magnitude smaller than predicted by the present steady-state theory.

We now let α_0 run through the interval $1° \leqslant \alpha_0 \leqslant 60°$, while $h_x\omega_s/\omega = 0.25$ is kept constant. Choosing α_0 as the abscissa figure 10 is obtained (again the other input

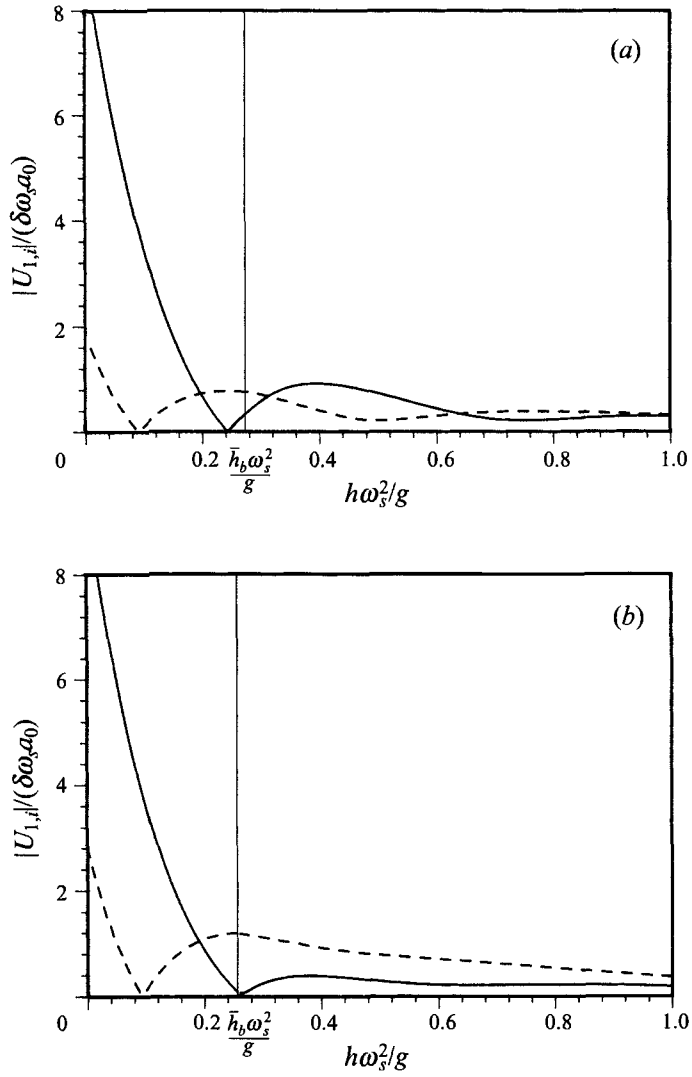

FIGURE 7. As figure 6 but for (*a*) $\alpha_0 = 30°$, and (*b*) $\alpha_0 = 45°$.

parameters were $\hat{h}_0 = 1$, $\hat{a}_0 = 0.1$, $\kappa = 1$, and $\gamma_0 = 0.4$). Clearly two different α_0-values are exceptional. One is $\alpha_0 = 53.1°$, which corresponds to the resonant forcing of edge waves of mode 1, and the other is $\alpha_0 = a_{cr} = 36.86°$, corresponding to the turning point from trapped to leaky modes. The peaks at $\alpha_0 = 53.1°$ only appear finite because the resolution of the abscissa is just 1°. An exception is the range $36.0° \leqslant \alpha_0 \leqslant 37.0°$, where the equidistance is 10 times smaller (only 0.1°). Contrary to the peaks at $\alpha_0 = 53.1°$, the peaks at $\alpha_0 = a_{cr} = 36.86°$ do *not* correspond to a singular infragravity-wave solution. In fact at $\alpha_0 = \alpha_{cr}$ where also $\lambda = 0$ and $\hat{h}_c = \hat{h}_0$, it appears that R and $|\xi_f|/(\delta a_0)$ have local finite maxima. This seems reasonable, since at this point they are measured right at the caustic depth. It is more surprising to see that $|\xi_1(0)|/(\delta a_0)$ has a local minimum there. The author has not found an explanation for this.

Schäffer & Jonsson (1992) derived the shallow-water edge-wave dispersion relation for a plane slope with a shelf and illustrated the results as dispersion curves in the $(-a, z_0')$-plane. Since both $-a$ (46), and z_0', (47), can be uniquely derived from the input

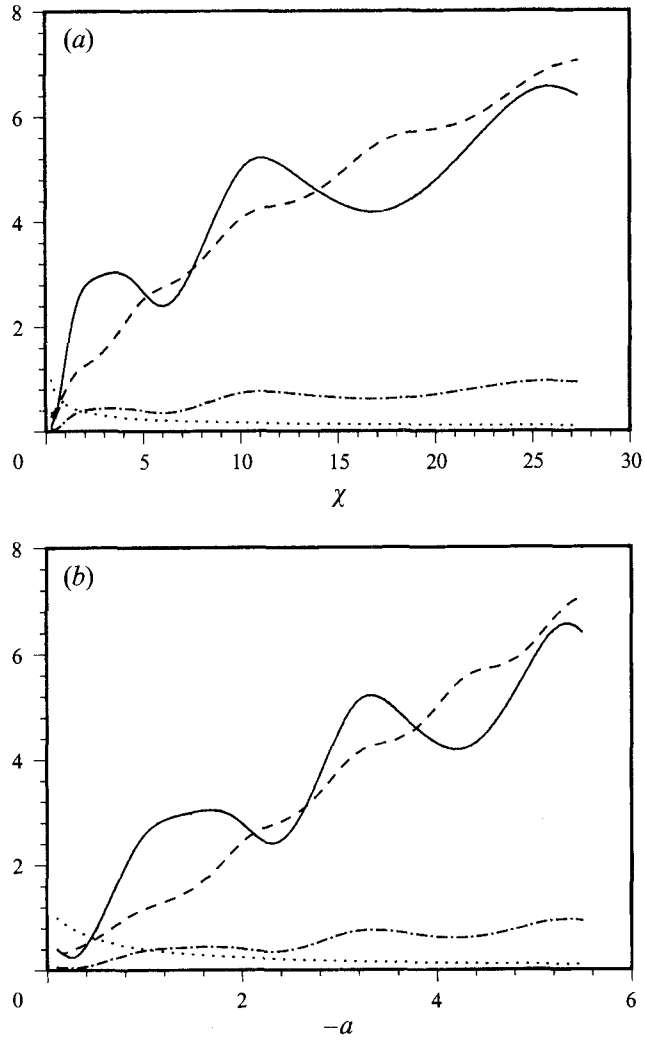

FIGURE 8. Two different representations of some key results for the infragravity-wave solution for a range of different values of the scaled beach slope, $0.1 \leqslant h_x\omega_s/\omega \leqslant 1.0$: ——, 'reflection coefficient' R; – – –, shoreline infragravity-wave amplitude, $|\xi_1(0)|/(\delta a_0)$; – · – · –, amplitude of the seaward progressing free long wave measured at the edge of the slope, $|\xi_f|/(\delta a_0)$. In (a) the abscissa is a derived 'relative phase' parameter $\chi \equiv (h_x\omega_s/\omega)^{-2}\hat{h}_b$ which is important for normally incident groups. In (b) the abscissa is the derived parameter $-a$ (see (18) and (48)) which is closely related to the edge-wave dispersion relation (figure 11) for the plane slope with a shelf (figure 1). the varied $h_x\omega_s/\omega$ (· · · · · ·) is shown in both graphs, and the other input parameters were kept constant at $\alpha_0 = 30°$, $\hat{h}_0 = 1$, $\hat{a}_0 = 0.1$, $\kappa = 1$, and $\gamma_0 = 0.4$.

parameters $h_x\omega_s/\omega$, α_0, and $\hat{h}_0$ (i.e. without finding the infragravity-wave solution) every set of input parameters corresponds to a point in the $(-a, z_0')$-plane. A variation of one of the input parameters thus gives a curve in the $(-a, z_0')$-plane which we shall denote a parameter path. Figure 11 gives the parameter paths for figures 8, 9(a), 9(b), and 10, also including the edge-wave dispersion curves from Schäffer & Jonsson (1992). For $z_0' \to \infty$ the influence of the shelf vanishes and the free edge-wave dispersion relation reduces to the classical result $-a = n$, where $n = 0, 1, 2, \ldots$ is the edge-wave mode. Consider first the straight-line segments. These correspond to constant λ-values, and their extensions all run through $(-a, z_0') = (-\frac{1}{2}, 0)$, cf. (49). In the order of

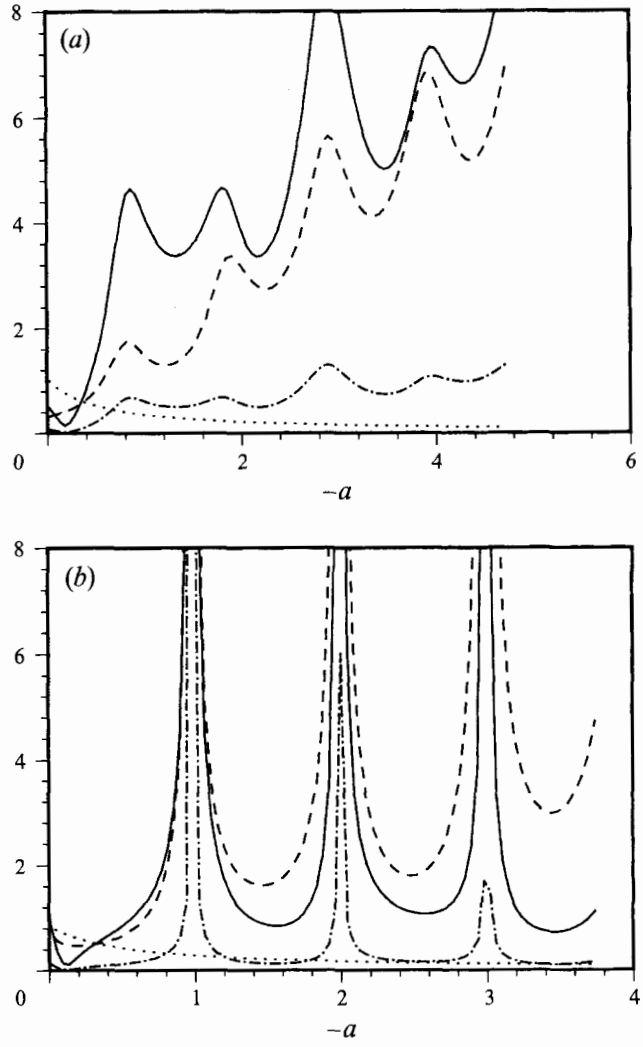

FIGURE 9. As figure 8(*b*) except for the angle of incidence α_0. In (*a*) $\alpha_0 = 35°$, close to the critical angle $\alpha_{cr} = 36.86°$ where trapping occurs, and near-resonant amplification shows in the peaks near integer values of $-a$. In (*b*) $\alpha_0 = 45°$ exceeds α_{cr} and edge-wave resonance occurs.

increasing slope (measured in the $(-a, z_0')$-system) these lines are given by $\lambda = -0.439$, -0.094, and 0.280. For $\hat{h}_0 = 1$, these values further correspond to $\alpha_0 = 30°$, 35°, and 45° as used in figures 8(*a*, *b*), 9(*a*), and 9(*b*), respectively.

In figure 11 the parameter path (dash-dot line) is not very close to the dispersion curves (solid line) and consequently the maxima (of e.g. *R*) corresponding to figure 8(*b*) show no correlation with near-integer values of $-a$.

The steeper line segment (dash-double-dot line) of figure 11 runs much closer to the dispersion curves, and at the $-a$-values where the distance is smallest marked peaks appear in the corresponding figure 9(*a*). Note that for the smaller $-a$-values the deviation from integer values in the dispersion curves of figure 11 (owing to the presence of the shelf) is also recognized in the lower peaks of figure 9(*a*).

The steepest line segment (dashed line) of figure 11 runs right through the dispersion curves, and the corresponding singularities evolve in figure 9(*b*).

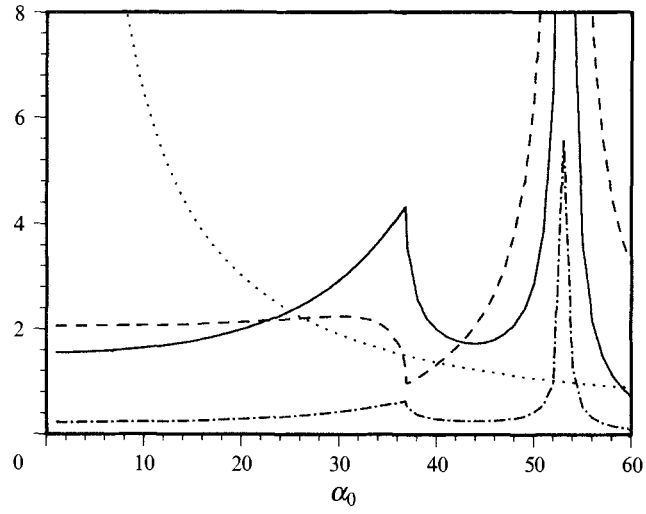

FIGURE 10. Some key results for the infragravity-wave solution versus the angle of incidence, $1° \leqslant \alpha_0 \leqslant 60°$: ——, 'reflection coefficient' R; – – –, shoreline infragravity-wave amplitude, $|\xi_1(0)|/(\delta a_0)$; – · – · –, amplitude of the seaward progressing free long wave measured at the edge of the slope, $|\xi_f|/(\delta a_0)$. The other input parameters were $h_x \omega_s/\omega = 0.25$, $\hat{h}_0 = 1$, $\hat{a}_0 = 0.1$, $\kappa = 1$, and $\gamma_0 = 0.4$. Also the derived parameter $-a$ (·····) is shown. Note the special behaviour at the critical angle of incidence $\alpha_{cr} = 36.86°$ and the edge-wave resonance at $\alpha_0 = 51.11°$.

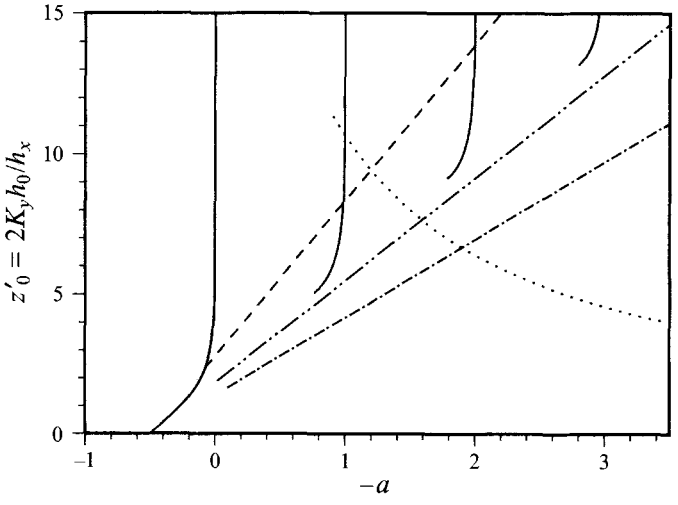

FIGURE 11. Parameter paths corresponding to figure 8 (a, b) (– · – · –) for which $(\lambda, \alpha_0) = (-0.439, 30°)$, figure 9 ($a$) (— · ·) for which $(\lambda, \alpha_0) = (-0.094, 35°)$, figure 9 ($b$) (– – –) for which $(\lambda, \alpha_0) = (0.280, 45°)$, and figure 10 (·····), for which $h_x \omega_s/\omega = 0.25$. The edge wave dispersion curves (——) valid for a plane slope connected with a shallow shelf are also shown, see Schäffer & Jonsson (1992).

Finally we consider the curve segment (dotted line) of figure 11, corresponding to figure 10, which from (46) and (47) is seen to be a segment of a hyperbola with asymptotes given by $z'_0 = 0$ and $-a = -\frac{1}{2}$. Again the crossing of a dispersion curve results in a singularity, cf. the peak at $\alpha_0 = 53.1°$ in figure 10. Furthermore, the intersection between the hyperbola segment and the caustic for the dispersion curves (the common tangent to the curved ends of the dispersion curves, not shown in the figure) is reflected in the finite peak at $\alpha_0 = \alpha_{cr} = 36.86°$ in figure 10. At this point also

$\lambda = 0$ and $\hat{h}_c = \hat{h}_0$. The hyperbola segment could have been extended upwards by increasing α_0 to values higher than 60° (as taken from the limit in figure 9), but the limit would be $\alpha_0 = 90°$ corresponding to $(-a, z_0') = (0.70, 13.34)$, indicating that for the particular $h_x \omega_s/\omega = 0.25$ and $\hat{h}_0 = 1.0$ the lowest edge-wave mode could not be excited. This would require a higher value of $h_x \omega_s/\omega$.

Imagine R, $|\xi_1(0)|/(\delta a_0)$, and $|\xi_f|/(\delta a_0)$ computed for varying sets of $(h_x \omega_s/\omega, \alpha_0)$. This would result in a surface, which could be depicted over the $(-a, z_0')$-plane. Figures 8(*b*), 9(*a*), 9(*b*) and 10 now represent four vertical sections of this surface, and the traces of these sections are the three line segments and the hyperbola segment of figure 11.

5. Summary

This work is a sequel to Schäffer (1993). That paper was concerned with the development of a mathematical model for the generation of infragravity waves over a one-dimensional topography by normally or obliquely incident groups of primary waves. Solutions for slightly modulated primary waves of normal incidence on a plane sloping beach were presented, with emphasis on the so-called dynamic set-down and set-up due to the incident bound long wave and to the oscillations of the break-point position, respectively. These phenomena are also relevant in the present paper which takes up the case of obliquely incident groups. Again the solution presented is restricted to small primary-wave modulation and a plane sloping beach. The new feature of the solution is the possibility of infragravity-wave trapping an edge-wave resonance. The occurrence of both these phenomena can be predicted from the input parameters without finding the infragravity-wave solution. Near-resonant edge-wave conditions are shown to result in amplification of the infragravity waves, as could be expected. A continuous variation of the angle of incidence shows that at the transition between trapped and leaky infragravity-wave modes, corresponding to a *cut-off* frequency, the solution shows a finite peak in the dimensionless infragravity-wave amplitude. This peak appears as a local maximum at the edge of the slope and as a local minimum at the shoreline, and the finite values indicate that no resonance occurs at the cut-off.

Professor I. G. Jonsson is gratefully acknowledged for stimulating discussions and comments, and for his help with the preparation of this manuscript. Furthermore, I am indebted to Professor I. A. Svendsen, who initiated the present research. This work was conducted while the author was a PhD student at the Institute of Hydrodynamics and Hydraulic Engineering (ISVA), Technical University of Denmark.

Appendix. Confluent hypergeometric functions

The *confluent hypergeometric equation*, also called *Kummer's equation*, reads

$$z' \frac{\partial^2 \Psi}{\partial z'^2} + (b - z') \frac{\partial \Psi}{\partial z'} - a\Psi = 0 \tag{A 1}$$

(see e.g. Abramowitz & Stegun 1972), where a and b are parameters. The two linear independent solutions are the Kummer functions (or confluent hypergeometric functions) the first and second kinds, M and U.

$$\Psi = M(a, b, z') \equiv \sum_{n=0}^{\infty} \frac{(a)_n}{n!(b)_n} z'^n, \tag{A 2}$$

where $(a)_n$ is *Pochhammer's symbol*:

$$(a)_n \equiv \frac{\Gamma(a+n)}{\Gamma(a)} = a(a+1)(a+2)\ldots(a+n-1) \tag{A 3}$$

and

$$\Psi = U(a,b,z') \equiv \frac{\pi}{\sin \pi b}\left\{\frac{M(a,b,z')}{\Gamma(1+a-b)\,\Gamma(b)} - z'^{1-b}\frac{M(1+a-b,2-b,z')}{\Gamma(a)\,\Gamma(2-b)}\right\}, \tag{A 4}$$

$$b \neq 0, \pm 1, \pm 2, \ldots, \quad a \neq 0, -1, -2, \ldots,$$

where Γ is the Gamma function. However, we need solutions for $b = 1$, since this corresponds to the long-wave equation (14). For integer values of b,

$$U(a,b,z') = U(a,n+1,z')$$

is defined (see Erdélyi 1953, equation (13), section 6.7, vol. 1):

$$\begin{aligned} U(a,n+1,z') \equiv \frac{(-1)^{n+1}}{n!\Gamma(a-n)}\Bigg\{&\ln z' M(a,n+1,z') \\ &+ \sum_{r=0}^{\infty}\frac{(a)_r z'^r}{(n+1)_r r!}[\psi(a+r)-\psi(1+r)-\psi(1+n+r)]\Bigg\} \\ &+ \frac{(n-1)!}{\Gamma(a)}\sum_{r=0}^{n-1}\frac{(a-n)_r}{(1-n)_r}\frac{z'^{r-n}}{r!}, \end{aligned} \tag{A 5}$$

$$a \neq 0, -1, -2, \ldots, \quad n = 0, 1, 2, \ldots,$$

where the last sum is to be omitted if $n = 0$, and ψ is the logarithmic derivative of the Γ-function (the *Digamma* function)

$$\psi(x) \equiv \frac{\mathrm{d}[\ln \Gamma(x)]}{\mathrm{d}x} = \frac{1}{\Gamma(x)}\frac{\mathrm{d}\Gamma(x)}{\mathrm{d}x}. \tag{A 6}$$

The Kummer function of the first kind is easily evaluated as

$$M(a,b,z') = \sum_{n=0}^{\infty} c_n z'^n, \tag{A 7}$$

where from (A 2)

$$c_{n+1} = c_n \frac{a+n}{(n+b)(n+1)}; \quad c_0 = 1. \tag{A 8}$$

This could also be found directly by inserting the series (A 7) in the differential equation (A 1).

The Kummer function of the second kind is more problematic, since we are particularly interested in the case $b = 1$, for which $U(a,b,z')$ is not defined when $a = -n$, $n = 0, 1, 2, \ldots$, corresponding to free edge waves on an infinite slope. Thus we seek a solution to (A 1) that is linearly independent of $M(a,b,z')$, and which is defined for $b = 1$ even when $a = -n$. Inspired by (A 5) we assume that a solution of the form

$$\Psi = U_m(a,b,z') \equiv \ln z' M(a,b,z') + T(a,b,z'), \tag{A 9}$$

where

$$T(a,b,z') = \sum_{n=0}^{\infty} d_n z'^n, \tag{A 10}$$

can be expected. Inserting (A 9) into (A 1) it follows that T must satisfy the inhomogeneous equation

$$z'\frac{\partial^2 T}{\partial z'^2}+(b-z')\frac{\partial T}{\partial z'}-aT=-2\frac{\partial M}{\partial z'}+\left(1+\frac{1-b}{z'}\right)M. \tag{A 11}$$

Now (A 10) inserted in (A 11) yields

$$(n+1)(b+n)\,d_{n+1}-(n+a)\,d_n-c_n+(b-1)\,c_{n+1}+2(n+1)\,c_{n+1}=0 \tag{A 12}$$

and

$$(b-1)\,c_0=0. \tag{A 13}$$

Thus it is only for $b=1$ that we can require $c_0=1$ and get a non-trivial solution $\Psi=M$. If $b\neq 1$, we have $c_0=0$, and the c_n-series sums up to $\Psi\equiv 0$, after which the d_n-series is simply $T=M$. Assuming that $b=1$ (which is the case we are interested in) yields

$$d_{n+1}=\frac{(a+n)\,d_n+c_n-2(n+1)\,c_{n+1}}{(n+1)^2}. \tag{A 14}$$

Since the c_n are known from (A 8), we can specify any d_0 and the rest of the d_n are given by (A 14). Thus $\Psi=U_m(a,1,z')$ given by (A 9) and (A 10) provides a solution to (A 1), which is linearly independent of $M(a,1,z')$ and valid even for $-a=0,1,2,\ldots$.

In the applications $M(a,1,z')$ and $U_m(a,1,z')$ were calculated numerically. M was checked against standard tables of confluent hypergeometric functions, and U_m was checked indirectly through an evaluation of the Wronskian of (M,U_m), invoking that according to the differential equation (A 1) we have (for $b=1$)

$$W(M,U_m)\propto\exp\left[-\int\frac{1-z'}{z'}\mathrm{d}z'\right]=\frac{\mathrm{e}^{z'}}{z'}. \tag{A 15}$$

REFERENCES

ABRAMOWITZ, M. & STEGUN, I. A. 1972 *Handbook of Mathematical Functions*. Dover.

BOWEN, A. J. & GUZA, R. R. 1978 Edge waves and surf beat. *J. Geophys. Res.* **83**, 1913–1920.

ECKART, C. 1951 Surface waves on water of variable depth. *Wave Rep.* 100. Scripps Inst. of Oceanogr., Univ. of California, La Jolla.

ERDÉLYI, A. 1953 *Higher Transcendental Functions*, vol. 1. McGraw-Hill.

FODA, M. A. & MEI, C. C. 1981 Nonlinear excitation of long-trapped waves by a group of short swells. *J. Fluid Mech.* **111**, 319–345.

GALLAGHER, B. 1971 Generation of surf beat by non-linear wave interactions. *J. Fluid Mech.* **49**, 1–20.

HUNTLEY, G. A., GUZA, R. T. & THORNTON, E. B. 1981 Field observations of surf beat. 1. Progressive edge waves. *J. Geophys. Res.* **86**, C7, 6451–6466.

LONGUET-HIGGINS, M. S. & STEWART, R. W. 1962 Radiation stress and mass transport in gravity waves with application to 'surf beats'. *J. Fluid Mech.* **13**, 481–504.

LONGUET-HIGGINS, M. S. & STEWART, R. W. 1964 Radiation stresses in water waves: A physical discussion with applications. *Deep-Sea Res.* **11**, 529–562.

MEI, C. C. & BENMOUSSA, C. 1984 Long waves induced by short-wave groups over an uneven bottom. *J. Fluid Mech.* **139**, 219–235.

MUNK, W. H., SNODGRASS, F. E. & CARRIER, G. F. 1956 Edge waves on the continental shelf. *Science* **123**, 127–132.

SCHÄFFER, H. A. 1990 Infragravity water waves induced by short-wave groups. *Series Paper* 50. Inst. Hydrodyn. Hydr. Eng. (ISVA), Techn. Univ. Denmark.

SCHÄFFER, H. A. 1993 Infragravity waves induced by short-wave groups. *J. Fluid Mech.* **247**, 551–588 (referred to herein as I).

SCHÄFFER, H. A. & JONSSON, I. G. 1992 Edge waves revisited. *Coastal Engng* **16**, 349–368.

SYMONDS, G., HUNTLEY, G. A. & BOWEN, A. J. 1982 Two dimensional surf beat: Long wave generation by a time-varying break point. *J. Geophys. Res.* **87**, C1, 492–498.